Vietnam Journal of Science and Technology ***64***(1) (2026) 100–113
DOI: https://doi.org/10.15625/2525-2518/21218

Strategies for thermal management in lithium-ion batteries: Mitigating thermal runaway risks

Srinivas Mallimoggala, K. Rama Devi

Electronics and Communication Engineering Department, College of Engineering Kakinada, Jawaharlal Nehru Technological University Kakinada, Andhra Pradesh, India

Emails: *mallimoggla@gmail.com; kolisettyramadevi@gmail.com*

Received: 26 July 2024; Accepted for publication: 28 March 2025

Abstract. Thermal runaway in lithium-ion batteries (LIBs) is currently one of the major safety concerns in high-energy applications that include electric vehicles, aerospace, and others. Thermal management especially must be well done to avert disastrous failures. This paper evaluates the use of aluminum as a heat spreader in controlling thermal runaway in a lithium-ion battery system with a 7s4p configuration using COMSOL Multiphysics. The thermal analysis of different cooling techniques is done in this work, examining air cooling and phase change material as well as the aluminum heat spreader concerning the peak temperature, heat removal, and thermal reliability. The analysis carried out on the results has shown that the use of aluminum heat spreaders greatly reduces the temperatures that reach their peak and improves heat spreading - facts that advocate for their effectiveness in increasing the thermal safety of lithium-ion battery packs.

Keywords: battery pack design, energy storage solutions, heat transfer modeling, COMSOL multiphysics, battery performance enhancement.

Classification numbers: 2.2, 2.8.

NOMENCLATURE

Symbol	Description and unit
General parameters	
SOC	State of charge
T	Temperature
t	Time (s)
x	Spatial coordinate (m)
r	Radial coordinate in spherical
ρ	Density (kg/m³)
c_p	Specific heat capacity at
k	Thermal conductivity
μ	Velocity vector (m/s)
τ	Characteristic time (s)
Electrical and electrochemical parameters	
E_{cell}	Cell voltage (V)
$E_{OCV}(SOC,T)$	Open circuit voltage (V)
η_{IR}	Overpotential due to internal
η_{act}	Activation overpotential (V)
I_{cell}	Current through the cell (A)
I_{1C}	Current corresponding to a
$Q_{cell,0}$	Nominal capacity of the
Thermal parameters	
Q_h	Total heat generation within
Q_{mix}	Heat generation due to
$E_{OCV,therm}$	Thermal component of the
$E_{OCV,ref}$	Reference OCV at a reference
T_{ref}	Reference temperature (C)
Other symbols	
∇	Nabla operator (vector)
$\cdot$	Dot product
Ω	Domain of integration

d_{vol}	Differential volume element	T_s	Temperature of the shell (K)
k_s	Shell's thermal conductivity	T_a	Ambient temperature (K)
h_{nat}	Natural convective heat	n	Direction normal to the

1. INTRODUCTION

Lithium-ion batteries are widely deployed in portable electronics, electric vehicles, aerospace, and industry due to high energy density, long cycle life, and rechargeability [1], yet they face serious safety risks from thermal runaway (TR) caused by overcharging, mechanical damage, manufacturing defects, high temperatures, electrical faults, and poor thermal management, requiring protection circuits and motivating safer alternatives such as lithium-sulfur, fluoride, and cobalt-free batteries.

Thermal runaway is a self-sustaining temperature escalation that occurs when heat generation exceeds dissipation capacity, initiating exothermic chain reactions that can lead to fires or explosions under abuse or faulty conditions [2].

Santos *et al.* [3] showed through COMSOL-based 3D electromagnetic analysis that variations in dielectric properties and magnetron frequency cause non-uniform heating and hot spots, triggering thermal runaway (TR) in microwave systems. Xu *et al.* [4] demonstrated via multiphysics simulation that combining liquid cooling with phase-change materials significantly suppresses TR propagation in lithium-ion batteries (LIBs), enhancing safety in high-energy applications. Dixon *et al.* [5] established through an electrochemical–thermal model that a temperature rise rate >1 °C/s and average temperature >80 °C markedly increase TR risk, enabling early detection strategies. Li *et al.* [6] confirmed experimentally and numerically that optimized liquid cooling coupled with appropriate insulation effectively limits TR spread in battery modules. Yang et al. [7] proved that integrating aerogels with liquid cooling plates offers superior TR mitigation compared to standalone methods in high-energy-density LIBs.

Rui *et al.* [8] developed a silica nanofiber–PCM smart firewall that effectively controls TR, highlighting advanced cooling materials for LIB safety. Feng *et al.* [9] found that phase-change materials outperform conventional insulation by slowing TR escalation and reducing post-transition thermal conductivity in next-generation LIBs. Zhang *et al.* [10] reported that interactions in hybrid energy storage systems (ESSs) aggravate TR, necessitating improved thermal management. Hossain Lipu *et al.* [11] showed that integrating multi-parameter TR detection into BMS significantly enhances early warning and prevention in electric vehicles

The main research question of this paper is therefore to assess the capability of aluminum as a heat spreader in preventing thermal runaway of lithium-ion battery packs. This research seeks to use the heat performance of aluminum to other cooling methods such as air cooling and phase change materials on peak temperature heat rejected, and thermal management stability of a 7s4p battery configuration. This work is specifically concerned with thermal control of Li-ion battery packs in high energy usage systems. The research conducts the thermal analysis of a 7s4p lithium-ion battery pack based on the research's conceptual design using COMSOL Multiphysics, evaluating the thermal performance of the battery pack under air cooling, phase-change material integration, and aluminum heat spreader. It encompasses a comparison of these cooling methods; the studies include the influence of these strategies on thermal runaway prevention, peak temperature, and thermal stability under different battery types and working conditions.

2. MODELING AND METHODOLOGY

The 7s4p (seven batteries in series and four such in parallel to give approximately 24 V 16 A) lithium battery packs are necessary in aviation and aerospace because of their high energy density and reliability, and flexibility of use, temperature stability, design, and standards compliance. These battery packs have a nominal voltage of 25.2 V and a large capacity, and can therefore be used for long flight times and reduced weight in drones and UAVs [12]. They also contain properties such as battery management systems, therefore can be useful in different uses. The working environment temperature of these battery packs is usually -20 °C to 60 °C, making them appropriate to conditions of aviation environment. The modeling and simulations are done with the assistance of an 'all in one' software known as 'COMSOL Multiphysics.' (hosted on a secure azure cloud and accessed through the I-STEM web portal).

Figure 1 shows a process for modeling and analyzing thermal management in lithium-ion battery packs and the risk of thermal runaway. Thus, it begins with battery pack shape and geometry as well as the thermal systems and events. The variation and heat interpolation scheme such as temperature, modality and conditions of the heat are established. It provides a true representation of the thermal system and simulates the working behaviors of the battery. Heat conduction, convection and radiation are caused, and boundary and initial conditions are stipulated for demonstrating safety threats of thermal runaway. The last step is the presentation of the result by visualizing and analyzing the outcome of the study.

2.1. Geometry and battery parameters

The details of vital parameters in the simulation and analysis of the lithium-ion battery pack are principally summarized in Table 1. It includes electric specifications, geometry, cooling plates geometry, layout, thermal properties, and initial state. To evaluate battery energy storage, nominal voltage, full charge voltage, and capacity of battery pack are required. Other physical measures of battery are based on the diameter of the battery, terminal thickness, and dimensions of the connector.

The cooling plates are of particular importance for controlling thermal properties of battery pack. The staking of the battery cells in the pack is also considered, the number of plates in one direction or the other. Other thermal properties of the battery pack are also considered, for example, the heat conductivity factor, density, and specific heat. The conditions upon which the simulation begins are set at 298.15 K (25 °C); and where the parameters characterizing the electrochemical processes described below are given at the reference temperature. The battery volume is given as 1.65E-05 m^3, and the trigger temperature for thermal events as 333.15 K (60 °C).

2.2. Boundary and initial conditions

Regarding the present investigation of thermal modelling of a 7s4p lithium-ion battery configuration, each of the variables stated in Table 1. has been explained in detail regarding each cell of the battery pack.

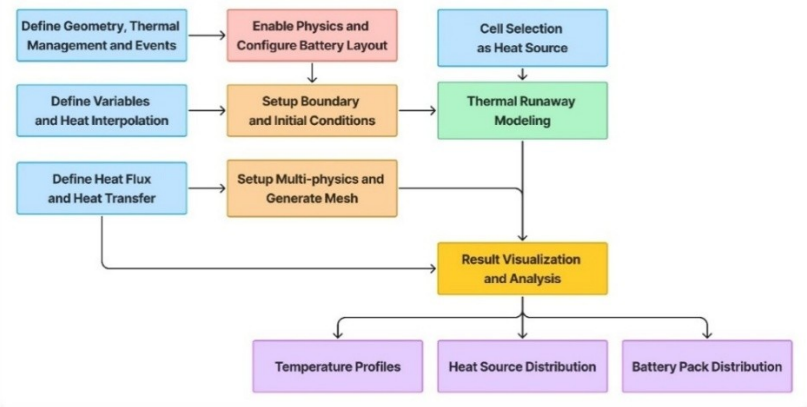

Figure 1. Flowchart for battery pack simulation process in COMSOL.

Table 2. Battery pack parameters and configurations for modeling.

Category	Parameters (Symbol = Value [Unit])
Battery Metrics	Nominal voltage = 25.6 V; Full charge voltage = 29.4 V; Capacity = 16 Ah
Cell Geometry (mm)	d_batt = 18; r_batt = 9; h_batt = 65; h_term = 1; r_term = 3; d_sc = 3; h_sc = 1; w_pc = 1; h_pc = 0.5
Cooling Plates (mm)	cp_wdh_mbs = 9×99×65; cp_wdh_mbp = 180×9×65
Layout	nx_batt = 7; ny_batt = 4; nx_plat = 6; ny_plat = 3
Thermal Properties	kT_batt_ang = 30 W/m·K; kT_batt_r = 1 W/m·K; ρ_batt = 2000 kg/m³; Cp_batt = 1400 J/kg·K; Ht = Ht_top = Ht_bottom = 30 W/m²·K
Initial & Trigger Conditions	T0 = T_init = 298.15 K; J0_0 = 0.85 A/m²; τ0 = 1000 s; η1C = 0.0045 V; V_batt = 1.654E-5 m³; T_avg_trigger = 333.15 K

This approach allows all the physical, electrical, and thermal parameters for every battery cell to be correctly recorded throughout the whole battery. The generation of heat across the cells is interpolated, it gives a very realistic simulation as to heat generation and dissipation across the pack. This is an important step because it considers the different ratings of the cell in terms of heat production from one operation condition to the other.

After the definition of the variables and heat interpolation for each battery in the pack, including surface and terminal region boundaries. This allows for a precision control and measurement of the heat exchange at these locations where heat exchange can dramatically change. From this, it is possible to accurately simulate the maximum and average temperatures of batteries in the pack, should one take time to consider the average battery pack temperature. This consideration is crucial with a view of finding out the aggregate thermal characteristics of the battery pack and come up with the hot spots that are likely to lead to thermal runaway.

To achieve this, the required boundaries and a cylindrical spatial frame work are set out. These limits help to define the real physical conditions to which the thermal model of the battery pack should correspond. Of course, if for example the frame is cylindrical, it is connected in geometry with cells, which can influence the appearance of a more realistic picture of distribution and heat transfer. Last but not the least, the initial condition of the model is chosen to be presented in Table 1 to present the thermal analysis.

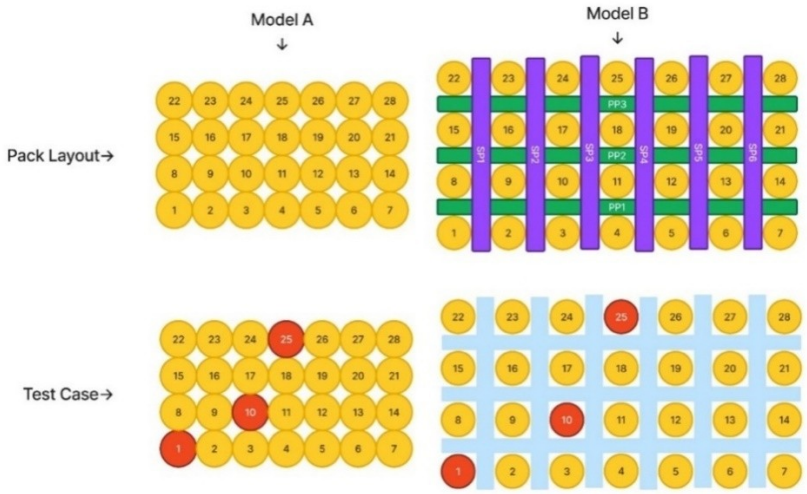

Figure 2. Schematic layouts and test cells of battery pack configurations: Models A and B.

Such conditions include other features like reference temperature, initial temperature as well as the specific electrochemical characteristics of the cells at the commencement of the simulation period. With these initial conditions set-up, the model is then ready to predict the thermal response of the 7s4p configuration in different operational conditions and to offer significant information about the pack's performance and safety.

2.3. Layout configuration and material properties

Figure 2 shows two layouts of the pack regarding battery configuration which has been labeled as model A and model B, also there is a depiction of the test cases for thermal analysis. These layouts and test cases are intended to observe and analyze the thermal profile of the battery pack under its normal operational parameters, and during thermal runaway.

2.3.1. Layout configuration

Model A (Straight pack configuration): Battery cells are tightly arranged adjacent to each other with minimal or no gaps or cooling plates, resulting in compact packing but poor heat dissipation and higher risk of heat accumulation under stress. Model B (Grid configuration with cooling plates): Battery cells are arranged in a grid integrated with cooling plates (SP1–SP6 and PP1–PP3), enhancing heat dissipation, reducing localized overheating, and improving overall thermal management compared to the straight pack layout.2.3.2. Test case consideration

For thermal analysis, cells 1, 10, and 25 were selected in test cases 1, 2, and 3, respectively, across both configurations (Figure 2) to evaluate location-based heat dissipation under thermal runaway conditions. In Model B (grid configuration), cell 1 is adjacent to two cooling plates, enabling effective heat capture and limiting propagation to neighboring cells. Cell 10 is surrounded by four cooling plates, providing maximum cooling support and allowing assessment under higher thermal stress due to multi-directional heat dissipation. Cell 25 is positioned near three cooling plates, representing an intermediate condition that helps evaluate the minimum cooling requirement needed to prevent thermal runaway while maintaining adequate heat dissipation.

2.3.3. Mesh and geometric construction

In this study, characteristics of a free tetrahedral mesh to be adopted in simulation for the four proposed models of battery packs (A and B) are enumerated as follows: This data is useful for evaluating the quality and the fineness of the mesh needed for the FEM simulations which are very useful in computational analysis of phenomena that occur in the battery packs.

Among the mesh types that are used are: vertices, tetrahedra, triangles, edge elements, vertex elements, minimum element quality, average element quality, element volume ratio, mesh volume, space dimension, domains, boundaries, edges, and vertices. The quality of the mesh affects and simulation of results and the lower and average elements affect the bearing stability and accuracy of it. The number of nodes must be equal to the size of the model object, the size dimension must be set to 3. There is also counting of the number of domains, boundaries and the like which also aids in creating a mesh with improved details.

Table 3. Comparison of mesh characteristics and quality metrics across models A and B.

Category	Metrics	Model A	Model B
Mesh size	Vertices	52,554	54,316
	Tetrahedra (= No. of elements)	291,782	304,479
	Triangles	68,149	75,108
	Edge elements / Vertex elements	8,276 / 1,386	12,021 / 1,704
Mesh quality & volume	Min quality / Avg quality	0.04949 / 0.5787	0.01485 / 0.5617
	Element volume ratio	5.75E−04	3.40E−04
	Mesh volume (m^3)	6.339E−4	1.242E−3
Geometry (3D)	Domains / boundaries	223 / 1,417	224 / 1,750
	Edges / vertices	2,068 / 1,386	3,328 / 1,704

The characteristics of a battery arrangement type 7s4p with LIB elements and their thermal characteristics are tabulated in Table 3. Because of their excellent heat transfer characteristics and high density, aluminum is preferred over other materials to use in absorption and dissipation of heat levels. The active battery, lithium-ion, is described by some unique thermal parameters such as heat capacity at constant pressure, thermal conductivity, density, etc. These properties are even more significant for reproducing inside temperature gradients as well as for the prediction of thermal runaway in case of thermal stress or runaway.

Figure 3 presents a comparison of two battery pack models, model A and model B, through four stages of design and analysis: Housing design refers to the structure and the outer cover for a battery pack; model refers to the design of the connecting network of batteries, active batteries in pack refer to batteries in a pack that are involved in a charging or a discharge process; cooling design refers to design of battery pack housing with view to ensuring that a battery is cooled. Housing of model A is quite simple with very little space between components which makes issues related to heat dissipation evident. Model B is structurally more complex, but obtained from model A with slight variations, hence the assumption that the designers have adopted a better strategy of handling heat is well founded. Mesh design is the design of the computational grid showing the discretized nature of the thermal and electrical behavior of the battery pack.

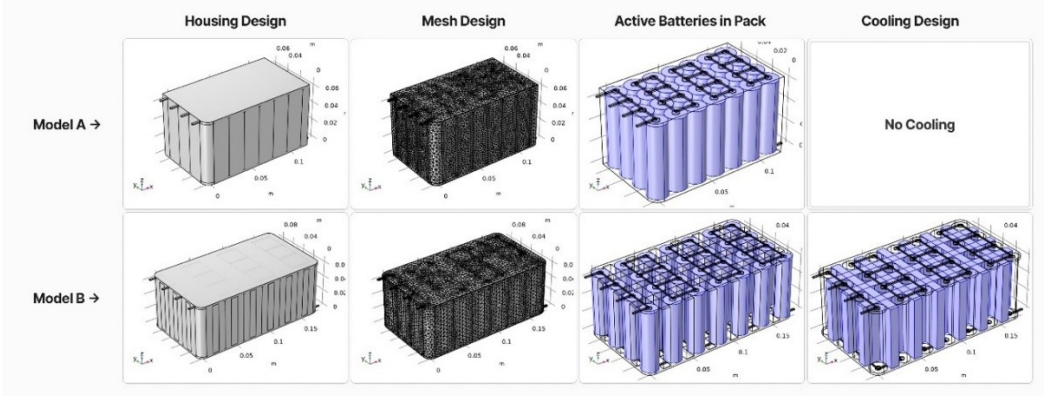

Figure 3. Comparison of battery pack configurations and cooling designs.

It has been observed that cells packed like shown in model A may encounter problems in heatsink while model B arrangement permits cooling air or fluid to pass around the cells dealing with the issue of thermal runaway.

Table 4. Material properties for model used in battery pack models.

Condition	Material	Heat capacity at constant pressure (J/kg·K)	Thermal conductivity (W/m·K)	Density (kg/m³)
Battery terminals	Aluminum	900	238	2700
Active battery	lithium- ion	Cp_batt	kT_batt_ang	rho_batt
Cooling model A	7s4p Straight configuration without cooling			
Cooling model B1	Air	1005	0.026	1.225
Cooling model B2	Paraffin solid	1850	0.4	861
Cooling model B3	Aluminum	900	238	2700

We can also see that in Table 3, the 7s4p straight configuration without cooling is a no cooling situation in which all heat dissipation is done by battery conduction, convection, and radiation. In cooling model B1 air as the cooling medium but it has a high heat capacity and low heat conductivity. Model B2 employs paraffin solid as its phase change material; it has high heat capacity though incredibly low thermal conductivity. Model B3 incorporates aluminum, the same as the battery terminals; the material has high thermal conductivity and average heat capacity. The high density of aluminum is beneficial as it increases the battery pack's weight, though this may be a disadvantage in some uses.

2.4. Multiphysics and mathematical model

The mathematical model for the 7s4p battery pack was constructed with the help of following equations and mathematical model design. The heat conduction equation (1) and extended heat conduction with convection (2) are crucial for understanding battery thermal behavior over time. The heat generation (3) Term breaks down heat sources within the battery, including resistive losses, electrochemical reactions, and reversible heat due to temperature-dependent changes in the open-circuit voltage, predicting battery operation heat generation [13-15].

$$\rho c_p \frac{\partial T}{\partial t} = \nabla \cdot (k\nabla T) + Q_h \quad (1)\ ; \qquad \rho c_p \frac{\partial T}{\partial t} + \rho c_p \mu \cdot \nabla T = \nabla \cdot (k\nabla T) + Q_h \quad (2)$$

$$Q_h = \left(\eta_{IR} + \eta_{act} + T \frac{\partial E_{OCV}(SOC|_{X=1,T})}{\partial T}\right) \ I_{cell} + Q_{mix} \quad (3)$$

The heat mixing term (4) in a battery for heat generated by variations in the state of charge, while the thermal dependence of open-circuit voltage (5) explains temperature-dependent changes in heat generation. The heat flux boundary condition (6) model explains heat transfer from the battery surface to the environment [16, 17].

$$Q_{mix} = \frac{3Q_{cell}}{\tau} \int_0^1 \left(\frac{\partial E_{OCV,therm}}{\partial SOC} \frac{\partial SOC}{\partial x} \frac{\partial SOC}{\partial x} x^2 dx\right) \quad (4)$$

$$E_{OCV,therm} = E_{OCV,ref}(SOC) - T_{ref} \frac{\partial E_{OCV}(SOC)}{\partial T} \quad (5)\ ; \quad -k_s \frac{\partial T}{\partial n} = h_{nat}(T_s - T_a) \quad (6)$$

The heat conduction (7) equation describes heat flow within a battery with temperature differences, while convective heat transfer at boundary (8) models heat removal through convection. The reiteration heat conduction equation (9) combines heat conduction, internal generation, and boundary conditions to capture all thermal dynamics [18-21].

$$q = -k\nabla T \ (7); \qquad q_{conv} = h(T_s - T_a) \ (8); \quad \rho c_p \frac{\partial T}{\partial t} = \nabla \cdot (k\nabla T) + Q_h \quad (9)$$

3. RESULTS AND DISCUSSION

Thermal runaway is mimicked through testing of certain cells in the battery pack, for instance test case 1, 2, 3 (Cell 1, Cell 10, Cell 25) among others. The simulation is initiated by creating a thermal runaway condition, with consequent temperature and pressure fluctuation. The battery pack responds, in terms of its understanding of heat transfer and potentially cascading failures. Post event, diagnostic scans are run and conducted to evaluate the battery pack and risks of damage or failure, structural design as well as protective measures. Comparing results allows to predict cells that might be at risk of what is called a catastrophic failure and to use this knowledge in designing safety and reliability concerning battery packs under severe conditions.

Tables 4 and 5 report the thermal analysis of various battery pack configurations considering the important parameters like peak temperature, average temperature and heat source characteristics based on distinguished cases instance test case 1, 2, 3 (Cell 1, Cell 10, Cell 25). Figures 4, 5 and 6 strengthen this data – the graphics of temperature and heat source over the indicated period clearly illustrate the thermal behavior described in the tables (Tables 4 and 5).

Table 4 gives vital information to do with peak temperature and heat source parameters concerned with various materials and set ups. The configuration of straight pack appears again and again to have the highest utmost temperatures across all the cases as 788.18 °C were recorded during case 1 and 883.69 °C in case 2. As it is further ascertained in Figure 4, the temperature curves for the straight pack (the red lines) are staying notably higher compared to the other materials. This visualization is useful for quick time integration and facilitates the understanding of the contrast in the top of the loop between configurations.

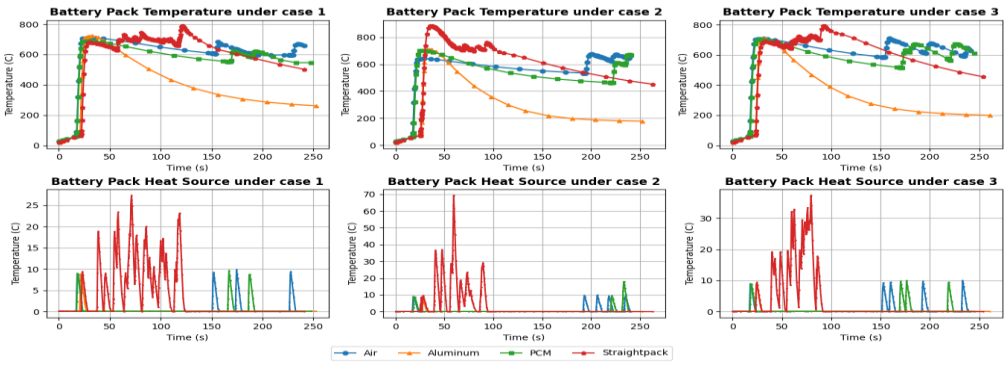

Figure 4. Temperature and heat source profiles of battery pack for all test cases.

To facilitate the analysis of the case studies, Figure 5 shows a bar graph on the temperature comparison of case 1, case 2 and case 3 with reference to four materials: air, straight pack, PCM and aluminum. The graphs depict the temperatures which feature in the different cases for the various material combinations and portray the fluctuations in thermal characteristics of the materials exposed to similar conditions.

The straight pack configuration demonstrates achieving maximum temperature; this is depicted on the graph in Figure 4 by the rise in the temperature curves. On the other hand, as observed from Figure 4, while the charts for the performance of air and PCM ascend more steeply and achieve their peak temperature gradually, the levels stabilize quickly. This could mean better ability to respond to these materials at high and low temperatures, the data in Table 4 supports this argument.

This comparison of heat sources of three different cases (case 1, case 2, and case 3) is presented in Figure 6 for four different materials, namely air, straight pack, PCM, and aluminum. The heat source time graphs illustrate fluctuation in the heat regarding the material configuration during operation of the battery packs under certain conditions emphasizing heat intensity and frequency. To compare the differences in thermal energy management of the materials, this figure is quite useful.

Table 4 illustrates that the straight pack has the highest of all the results regarding the peak heat source, 69.403 °C in case 1. These high peaks are evident when one looks at the heat source graphs in Figure 4 and Figure 5, where the straight pack group has revealed many and high peaks showing that heat energy is greatly located in this group. In contrast to that, the PCM and aluminum have much lower values of peak heat sources in the table, which is in concordance with the weak and steady heat source curves in Figure 4.

The metrics of Table 5 elaborate of the existence of another layer furnishing the average, the minimal, the maximal and the final temperature of every configuration. In the present case we can see that the average temperature is lower for PCM and aluminum and hence the case indicates that these two materials can provide more stable temperature. For instance, in case 1 of the research, the average temperature of PCM is 488.683 °C, compared to 653.388 °C for straight-pack. This stability is best illustrated in Figure 4 where the curves of the PCM temperature (in orange) are lower and are less fluctuating with time.

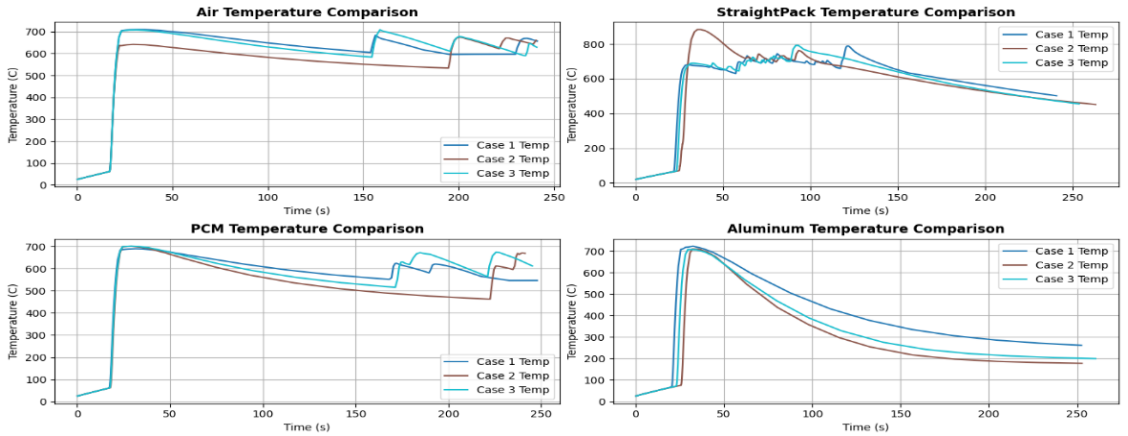

Figure 5. Temperature profiles under model consideration.

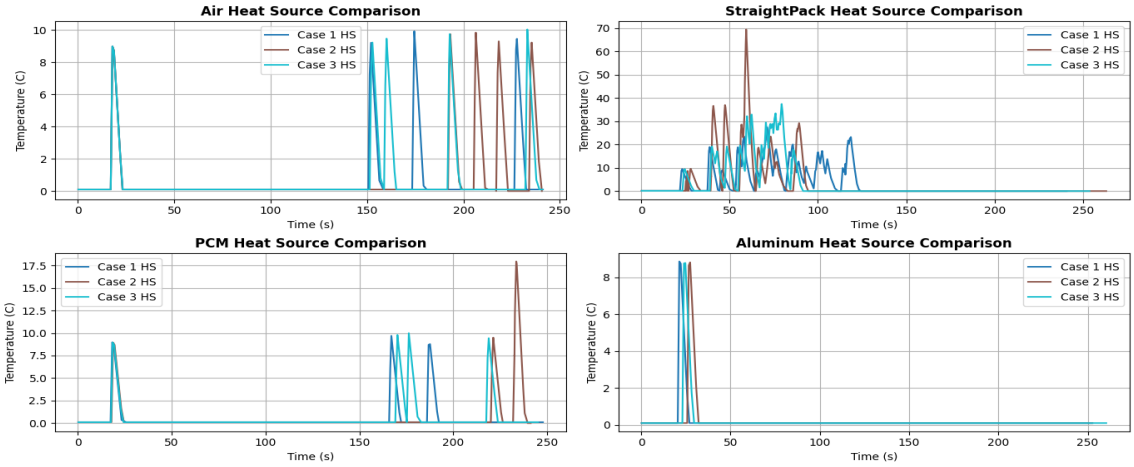

Figure 6. Heat source under model consideration.

Table 5. Comparison of peak temperature and heat source with time.

Case	Metric	A–Straight	B1–Air	B2–PCM	B3–Al
1 (C1)	Peak T (°C)	788.18	709.6	689.1	723.13
	Time @ Peak T (s)	120.95	31.507	31.379	32.509
	Peak Heat	27.398	9.9243	9.6982	8.8541
	Time @ Peak Heat (s)	71.308	174.47	167.03	21.318
2 (C10)	Peak T (°C)	883.69	674.65	700.25	710.11
	Time @ Peak T (s)	37.14	200.81	29.311	32.133
	Peak Heat	69.403	9.843	17.964	8.8056
	Time @ Peak Heat (s)	59.38	206.39	233.58	27.369
3 (C25)	Peak T (°C)	791.99	708.09	700.82	707.26
	Time @ Peak T (s)	93.105	158.8	29.235	29.599
	Peak Heat	37.383	10.038	9.9945	8.7697
	Time @ Peak Heat (s)	79.446	233.1	176.33	24.679

Table 6. Comparison of average, minimum, maximum and final pack temperatures in °C for all models.

Case	Metric	A–Straight	B1–Air	B2–PCM	B3–Al
1 (C1)	Avg	653.388	534.8646	488.6832	345.0898
	Min	25.001	25.001	25.001	25.001
	Max	788.18	709.6	689.1	723.13
	Final	502.13	656.61	546.23	261.57
2 (C10)	Avg	665.9065	544.7768	488.6504	304.9047
	Min	25.001	25.001	25.001	25.001
	Max	883.69	674.65	700.25	710.11
	Final	451.74	660.48	668.56	177.6
3 (C25)	Avg	641.3342	555.4983	511.1222	311.9852
	Min	25.001	25.001	25.001	25.001
	Max	791.99	708.09	700.82	707.26
	Final	455.06	628.7	611.79	199.6

The maximum temperatures to compare with the peak values in Table 5 show that the straight pack realizes the highest thermal values. Here, as can be seen in Figure 4, the maximum temperatures of these products are clearly shown, where the red line corresponding to the straight pack evidences peaks beyond all the other products. This picture echoes the notion that during use at high temperatures, the straight pack might become a danger of overheating over long-term operation.

Last pack temperatures presented in Table 5 give a glimpse of the heat that is likely to be left in the battery pack after the simulation time elapses. In these cases, metallic foams like PCM, and aluminum present low final pack temperature, for example 199.6 °C for aluminum in case 3.

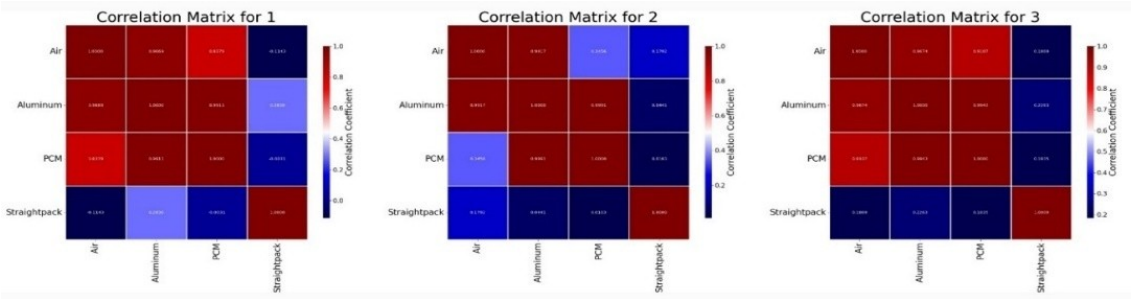

Figure 7. Correlation matrix of heat source considered.

Figure 4 also assists in understanding such a cooling trend: while the two temperature curves characteristic of PCM and aluminum are smoother and less steep compared to the straight pack, they steep up more slowly, this means that these materials not only regulate heat during use but also discharge heat faster after use, thereby minimizing the incidence of thermal runaway in the next cycles. Figure 7 presents the correlation matrices representing the relationships between different materials (air, aluminum, PCM, and straight pack) across three different cases, labeled as 1, 2, and 3.

In case 1, air and aluminum exhibit a very strong positive correlation (0.967), air and PCM show moderate positive correlation (0.838), and air and straight pack display a weak negative relationship (−0.114); aluminum and PCM are almost perfectly correlated (0.991), aluminum and straight pack show weak positive correlation (0.283), while PCM and straight pack have

negligible negative association (−0.003). In case 2, air and aluminum correlation further strengthens (0.992), air and PCM weakens significantly (0.346), air and straight pack remains weak (0.179), aluminum and PCM remain nearly perfectly correlated (0.999), aluminum and straight pack is negligible (0.044), and PCM and straight pack remain insignificant (0.010). In case 3, air and aluminum remain strongly correlated (0.967), air and PCM become strongly positive (0.911), air and straight pack stay weak (0.187), aluminum and PCM remain highly correlated (0.994), aluminum and straight pack show weak association (0.226), and PCM and straight pack continue to exhibit low correlation (0.183). Figure 8 presents the temperature correlation matrices for air, aluminum, PCM, and straight pack across three cases. In case 1, PCM and straight pack show strong positive correlation with air, while aluminum exhibits a weaker yet significant relationship, indicating lower environmental sensitivity.

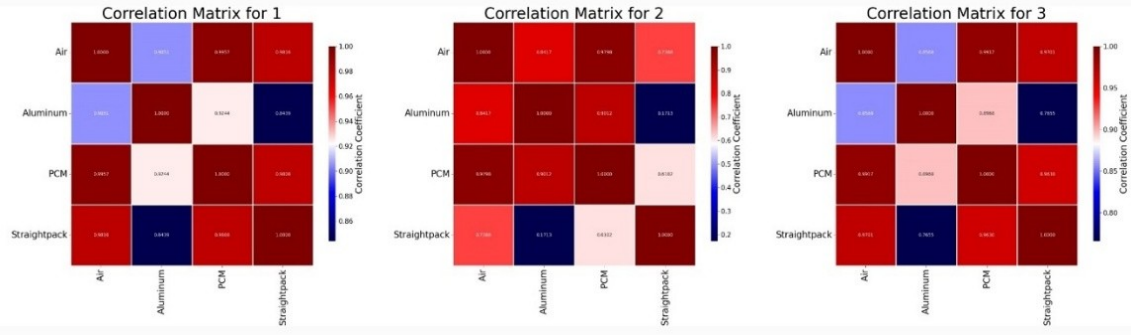

Figure 8. Correlation matrix of different battery pack configurations.

In case 2, air remains strongly correlated with PCM but shows reduced correlation with straight pack, and the aluminum–straight pack correlation becomes negligible, indicating minimal thermal interaction. In case 3, strong air correlations with PCM and straight pack reappear, aluminum's dependence on air improves compared to case 2 but remains weaker than the others, and its correlations with other materials stay moderate. Overall, air consistently dominates the thermal behavior of PCM and straight pack, whereas aluminum shows comparatively weaker and more variable thermal coupling. Figure 9 shows the distribution of an analyzed variable in 3 cases when using different modeling approaches (A, B1, B2, B3). We present model A which has a uniform distribution and three variants of model B, in which the high values are more concentrated in certain spatial areas, meaning that there can be differences in the underlying processes or effects inferred by each model. Since all the cases used in the analysis have similar patterns of values, the trends in the evaluation are stable, while the fluctuations between the models show the degree of localization and concentration in the data that was analyzed. The grid configuration with aluminum is the optimal one, but production may be more expensive and the battery pack size is a factor with its addition. This can be solved by proposing solutions like lightweight aluminum alloys, the use of advanced aluminum alloys with high strength-to-weight ratios would make the grid lighter without affecting performance, for example Al 6063-T83 & Al 3003-H18 (Corrosion resistance), both alloys have a good strength-to-weight ratio, which may assist in offsetting the increased weight problem.

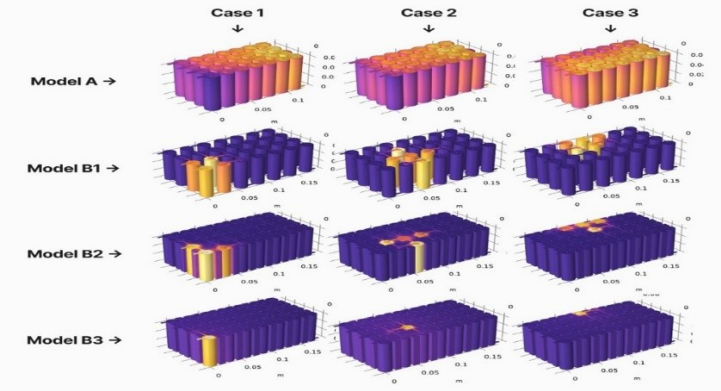

Figure 9. Comparison of heat profiles of all models and test cases.

4. CONCLUSIONS

The research proves that aluminum heat spreaders perform better than alternative configurations, including straight packs, air cooling, and PCM, in controlling thermal runaway hazards in lithium-ion battery packs. Aluminum recorded consistently lower peak temperatures - 723.13 °C, 710.11 °C, and 707.26 °C in three test cases - compared to the straight pack, which reached perilous peaks of 788.18 °C, 883.63 °C, and 791.99 °C. Moreover, aluminum provided a smooth decrease to dramatically lower final temperatures (e.g., 261.57 °C in case 1 compared to 502.13 °C for the straight pack). Its high thermal conductivity allowed for swift heat discharge, minimizing residual heat stress and hot spots. According to these findings, the most appropriate model for thermal management improvement, reliability assurance, and thermal runaway mitigation in high-energy battery systems is the aluminum heat spreader.

CRediT authorship contribution statement. Srinivas Mallimoggala: Conceptualization, Formal analysis, Methodology, Writing – original draft, Writing – review & editing. K. Rama Devi: Methodology, Supervision, Writing – review & editing.

Declaration of competing interest and funding. The authors declare that they have no known competing financial interests or personal relationships that could have appeared to influence the work reported in this paper. No funding from any agencies.

REFERENCES

1. U.S. Department of Energy - How lithium-ion batteries work. https://www.energy.gov/energysaver/articles/how-lithium-ion-batteries-work (accessed 16 April 2024).
2. Wishart L. - A brief explanation of thermal runaway. https://lectromec.com/a-brief-explanation-of-thermal-runaway/ (accessed 16 April 2024).
3. Santos T., Costa L. C., Valente M., Monteiro J., Sousa J. - Proceedings of the COMSOL Conference 2010, (2010)
4. Xu H., Wu S., Chen Y., Luan W. - Simulation on the management of lithium-ion batteries' thermal runaway via liquid cooling and phase change barrier. J. Phys. Conf. Ser., **2401**(1) (2022) 012019. https://doi.org/10.1088/1742-6596/2401/1/012019.
5. Dixon B., Mason A., Sahraei E. - Effects of electrolyte, loading rate and location of indentation on mechanical integrity of li-ion pouch cells. J. Power Sources, **396** (2018) 412-420. https://doi.org/10.1016/j.jpowsour.2018.06.042.

6. Li L., Xu C., Chang R., Yang C., Jia C., Wang L., Song J., Li Z., Zhang F., Fang B., Wei X., Wang H., Wu Q., Chen Z., He X., Feng X., Wu H., Ouyang M. - Thermal-responsive, super-strong, ultrathin firewalls for quenching thermal runaway in high-energy battery modules. Energy Storage Mater., **40** (2021) 329-336. https://doi.org/10.1016/j.ensm.2021.05.018.
7. Yang X., Duan Y., Feng X., Chen T., Xu C., Rui X., Ouyang M., Lu L., Han X., Ren D., Zhang Z., Li C., Gao S. - An experimental study on preventing thermal runaway propagation in lithium-ion battery module using aerogel and liquid cooling plate together. Fire Technol., **56**(6) (2020) 2579-2602. https://doi.org/10.1007/s10694-020-00995-x.
8. Rui X., Feng X., Wang H., Yang H., Zhang Y., Wan M., Wei Y., Ouyang M. - Synergistic effect of insulation and liquid cooling on mitigating the thermal runaway propagation in lithium-ion battery module. Appl. Therm. Eng., **199** (2021) 117521. https://doi.org/10.1016/j.applthermaleng.2021.117521.
9. Feng X., Lu L., Ouyang M., Li J., He X. - A 3D thermal runaway propagation model for a large format lithium ion battery module. Energy, **115** (2016) 194-208. https://doi.org/10.1016/j.energy.2016.08.094.
10. Zhang Y., Liu H., Li Z. - Thermal runaway in hybrid energy storage systems: challenges and mitigation strategies. J. Energy Storage, **15** (2022) 405-415.
11. Hossain Lipu M. S., Miah M. S., Ansari S., Wali S. B., Jamal T., Elavarasan R. M., Kumar S., Naushad Ali M. M., Sarker M. R., Aljanad A., Tan N. M. L. - Smart Battery Management Technology in Electric Vehicle Applications: Analytical and Technical Assessment toward Emerging Future Directions. Batteries, **8**(11) (2022) https://doi.org/10.3390/batteries8110219.
12. Haredata Electronics - 7S4P Lithium Ion Battery Pack: 25.2V 11.6Ah with SMBus. https://www.haredataelectronics.co.uk/7s4p-li-ion-battery-pack-25.2V-11.6Ah (accessed 16 April 2024).
13. Eddahech A., Briat O., Vinassa J.-M. - 2013 IEEE International Symposium on Industrial Electronics, IEEE, (2013) 1-5. https://doi.org/10.1109/ISIE.2013.6563807.
14. Maher K., Boumaiza A., Amin R. - Understanding the heat generation mechanisms and the interplay between joule heat and entropy effects as a function of state of charge in lithium-ion batteries. J. Power Sources, **623** (2024) https://doi.org/10.1016/j.jpowsour.2024.235504.
15. Liu G., Ouyang M., Lu L., Li J., Han X. - Analysis of the heat generation of lithium-ion battery during charging and discharging considering different influencing factors. J. Therm. Anal. Calorim., **116**(2) (2014) 1001-1010. https://doi.org/10.1007/s10973-013-3599-9.
16. Eddahech A., Briat O., Vinassa J.-M. - Thermal characterization of a high-power lithium-ion battery: Potentiometric and calorimetric measurement of entropy changes. Energy, **61** (2013) 432-439. https://doi.org/10.1016/j.energy.2013.09.028.
17. Hasan M., Khan M. Z. I., Biswas R., Islam N., Habibullah H., Afikuzzaman M. - Modeling of transient free convection flow in terms of permeability and thermal radiation. J. Therm. Anal. Calorim., **149**(12) (2024) 6551-6572. https://doi.org/10.1007/s10973-024-13145-0.
18. Mallimoggala S. - Advanced thermal management in aircraft lithium-ion battery packs: optimization of heat dissipation using heat spreaders and phase change materials. J. Therm. Eng., (2025) 1420-1438. https://doi.org/10.14744/thermal.0000984.
19. T'Jollyn I., Callewaert M., Nonneman J., Van de Wauw J., Ameel B., De Pacpe M. - 2019 18th IEEE Intersociety Conference on Thermal and Thermomechanical Phenomena in Electronic Systems (ITherm), IEEE, (2019) 1307-1312.
20. Aman S., Khan I., Ismail Z., Salleh M. Z., Al-Mdallal Q. M. - Heat transfer enhancement in free convection flow of CNTs Maxwell nanofluids with four different types of molecular liquids. Sci. Rep., **7**(1) (2017) 2445. https://doi.org/10.1038/s41598-017-01358-3.
21. Guo J., Guo Q., Liu J., Wang H. - The Polarization and Heat Generation Characteristics of Lithium-Ion Battery with Electric–Thermal Coupled Modeling. Batteries, 9(11) (2023) https://doi.org/10.3390/batteries9110529.